Biosynthesis of Calcium Hydroxylapatite Coating on Sputtered Ti/TiN Nano Multilayers and their Corrosion Behavior in Simulated Body Solution

BALASUBRAMANIAN SUBRAMANIAN,* PERUMAL DHANDAPANI, SUNDARAM MARUTHAMUTHU AND MUTHIRULANDI JAYACHANDRAN
Central Electrochemical Research Institute, Karaikudi 630006, India

ABSTRACT: Titanium/titanium nitride (Ti/TiN) nanoscale multilayered films were deposited onto 316L stainless steel substrates by reactive magnetron sputtering using a Ti target. Coatings characterized by X-ray diffraction showed that the stack possesses centered cubic structure. The X-ray photoelectron spectroscopy survey spectra on the etched surfaces of the stack film on steel exhibited the characteristic Ti2p, N1s, and O1s peaks at the corresponding binding energies 454.5, 397.0, and 530.6 eV, respectively. Platelet adhesion experiments were carried out to examine the interaction between blood and the materials *in vitro*. The results indicated that the smoothness and lower isoelectric point contribute to better hemocompatibility of the Ti/TiN nanoscale multilayered coating. The biomediated synthesis of calcium hydroxylapatite (HA) was carried out on coated substrates using calcium-depositing bacteria. The observation of low corrosion current density (I_{corr}) for the calcium HA-coated Ti/TiN specimens in simulated body fluid confirmed their highly resistive nature under the testing condition.

KEY WORDS: biofilm, corrosion, biocompatibility, hemocompatibility, hydroxylapatite coating.

*Author to whom correspondence should be addressed.
E-mail: subramanianb3@gmail.com
Figures 1, 3, 5 and 6 appear in color online: http://jba.sagepub.com

0885-3282/12/06 0687–19 $10.00/0 DOI: 10.1177/0885328210377534

INTRODUCTION

Stainless steel (SS) is the most commonly used material for dental implant applications. It possesses good corrosion resistance, but releases toxic metal ions, which lead to cell damage or failure of implants. This can be controlled by surface modification of implants by coating it with titanium nitride (TiN) [1]. TiN possesses excellent combination of properties, such as hardware performance, aesthetic appearance and contamination safety, and are used in making surgical tools and implants as well as food contact applications [2]. TiN coatings provide new possibilities for producing nontoxic and human fibroblast-compatible surface layer on Ti [3]. Fibroblast cells adhere more intimately to the surface of a TiN-coated Ti substrate compared with an uncoated Ti substrate [4]. TiN coatings, having good chemical stability, high hardness, excellent wear resistance, and intrinsic biocompatibility properties help avoid leaching of toxic elements. But Ti coating on bone implants is a failure due to the fact that titanium is much stiffer than bone and low level stress-shielded [5]. In recent years, even the failure of Ti/TiN-coated orthopedic prostheses was noticed [5]. Hydroxylapatite (HA) is a biocompatible and bioactive material that can be used to restore damaged calcified human tissues [6,7]. The major factors involved in both implant fixation and long-term stability are the coating resorption, bone in growth and mechanical fixation [7]. Several methods such as dip coating–sintering [8,9], immersion coating [10,11], electrophoretic deposition [12], solution deposition [13], ion-beam sputter coating [14], dynamic mixing [15], plasma spraying [16,17], flame spraying [18], and sol–gel have been involved in developing HA coatings [19]. Nowadays, biometic methods are involved for depositing calcium HA coating either on Ti or on TiN surfaces [20–23]. Calcium-precipitating bacteria (CPB) play a major role in forming calcium- and phosphate-accumulated cells in teeth pulp stones. Yong et al. [24] reported the synthesis of nanophase HA on *Serratia* sp. using $CaCl_2$ and inorganic phosphate. It is reported that the bacterial cell wall, containing more number of carboxylic groups, acts as the template for calcium nucleation sites to produce calcium HA, which shows excellent biocompatibility and is bioactive in the human body. It is highly compatible with various tissues and can adhere directly to osseous, soft, and muscular tissues without an intermediate layer of modified tissues [25,26].

In this study, we have synthesized calcium HA coatings through a biomediated method by using calcium-depositing bacteria. The corrosion behaviors of these coatings deposited on TiN- and Ti/TiN-coated AISI

316L SS substrates in simulated body solution by electrochemical methods were studied and the results are presented.

EXPERIMENTAL

Substrate Pretreatment

The SS substrate was used as 316L. Coupons of the substrate were cut to $50 \times 25\,mm^2$ in size and the surface was ground with SiC paper to remove oxides and other contamination. The polished substrates were degreased with acetone and then catholically electrocleaned in an alkaline solution containing sodium hydroxide and sodium carbonate for 2 min at 70°C, followed by rinsing with triple distilled water. These substrates were subsequently dipped in 5 vol.% H_2SO_4 solution for 1 min and thoroughly rinsed with distilled water.

Deposition of Ti/TiN and its Characterization

The layers of Ti and TiN were deposited on well-cleaned AISI 316L SS substrates using a reactive DC magnetron sputtering HIND HIVAC unit. The base vacuum of the chamber was below 10^{-6} Torr (1.33×10^{-4} Pa) and the substrate temperature was kept at 400°C. High purity argon was fed into the vacuum chamber for the plasma generation. High purity nitrogen was added as the reactive gas. The substrates were etched for 5 min using a DC power of 50 W in an argon pressure of 10^{-2} Torr (1.33 Pa). A high purity (>99.99%) Ti target of 5 cm diameter was used as the cathode. The multilayer films with controlled layer thickness were deposited using a dwell time controller. The substrate was moved back and forth between the two targets, using a stepper motor connected to the substrate to achieve multilayer deposition. The total number of layers was about 200 with bilayer thickness 80 Å. The total thickness of the film was 1.5 μm. The chemical nature of the outermost part of the film was obtained by X-ray photoelectron spectroscopy (XPS) using Multilab 2000. The XPS measurements were performed at a base pressure of 10^{-8} Torr with MgKα (X-ray of 1253.6 eV source). X-ray diffraction (XRD) was used to examine the changes in preferred grain orientation. XRD patterns were recorded using an X'pert pro diffractometer using CuK_α (1.541 Å) radiation from a 40 kV X-ray source running at 30 mA. The surface morphology of the coating was characterized by a Hitachi S 3000H microscope and a molecular imaging atomic force microscope (AFM). Transmission electron

microscopic (TEM) images were obtained using a 200 kV Tecnai-20 G2. For such measurements, the samples were suspended in acetone with ultrasonic dispersion for 3 min. Then a drop of this suspension was deposited on a holey carbon grid and then allowed for drying. TEM images of the samples were recorded both in the axial direction and in the perpendicular direction using a Multiscan CCD camera (model 794, Gatan) under low-dose conditions.

Biosynthesis of Calcium HA Film

Sample Collection

Fresh saliva samples were collected at 6.00 a.m. and calcified bacteria were isolated. Sterilized water was used to dilute the saliva sample, with the help of a sterile brush, in a well-cleaned sterilized container, stored in an ice box and then sent for microbiological characterization.

Isolation of Calcium-precipitating Bacteria from an Orthodontic Patient's Saliva Sample

The saliva sample was serially diluted using 9 mL of sterile distilled water. The total viable bacterial counts were enumerated by standard pour plate method using modified Mueller Hinton agar medium [27]. The composition of the modified Mueller Hinton agar medium is as follows: casein acid hydrolysate, 17.5 g/L; beef infusion, 2.0 g/L; starch soluble, 1.5 g/L; calcium chloride, 1 g/L; and agar, 20 g/L. The samples were mixed thoroughly and allowed to solidify. Then the inoculated plates were incubated at 37°C. Triplicates were also maintained. Total bacteria population was enumerated after 48–72 h of incubation, which was expressed as colony forming units per milliliter (CFU/mL).

Biomediated Synthesis of Calcium HA on TiN- and Ti/TiN-coated Substrates

Three hundred milliliters of modified Mueller Hinton broth were taken in a 500 mL clean conical flask. This broth was inoculated with 10 mL of CPB cultures. The coated coupons were immersed with broth under sterile condition and then placed in the incubator for 48 h at 37°C. After incubation, the coupons were removed from the medium. These specimens were twice washed with autoclave-distilled water to remove unattached bacteria, which were used for total viable count studies (to measure bacterial load on the metal surface). Then they were gently heated and air dried to get calcium HA (biofilm) formation on TiN and Ti/TiN coatings.

Epi-fluorescence Microscope Observation

The TiN- and Ti/TiN-coated specimens with biofilm were immersed for 5 min in 3% glutaraldehyde solution in order to fix the biofilm onto the coating surface. Then, the coupons were gently rinsed with autoclaved and sterilized distilled water and two drops of 0.01% aqueous solution of acridine orange were added. These samples were kept in the incubator for 15 min. The morphology of the biofilm was studied with a Nikon epi-fluorescence microscope: Model E200, Nikon, Tokyo, Japan.

Hemocompatibility Studies

Platelet adhesion experiments were carried out to evaluate surface thrombogenicity of the materials and to examine the interaction between blood and the materials *in vitro*. The specimen was washed and then incubated in human platelet-rich plasma (PRP) for 60 min at 37°C. After incubation, the specimens were fixed in glutaraldehyde and critical point dried followed by gold sputtering for examination using a scanning electron microscope.

Electrochemical Corrosion Studies

Conventional three-electrode cell assembly was used for polarization studies as well as for impedance measurements. Bare SS substrate, Ti/TiN-coated SS and biomediated synthesized calcium HA on Ti/TiN-coated specimens were used for analysis.

Electrochemical polarization studies were carried out with a PARSTAT electrochemical workstation. Experiments were conducted using the standard three-electrode configuration, with a platinum foil as the counter electrode, saturated calomel as the reference electrode and the sample as the working electrode. Specimen (1.0 cm^2 exposed area) was immersed in the test solution of modified Fusayama-simulated bodily fluid [28]. Experiments were carried out at room temperature (28°C). The system was allowed to attain a steady potential value for 10 min. The steady state polarization was carried out between −550 mV versus SCE from the open circuit potential (OCP) and +200 mV versus SCE from the OCP separately using distinct electrodes at a scan rate of 10 mV/s.

The specifications of electrodes were same for both polarization and impedance studies. In order to establish the OCP, prior to measurements, the sample was immersed in the solution for about 60 min. After attaining steady state, an alternate current (AC) signal of 10 mV amplitude was applied and the impedance values were measured in the frequency range between 0.01 Hz and 100 kHz.

RESULTS AND DISCUSSION

Surface Composition and Structure Analyses

On the surface of the Ti/TiN nanoscale multilayered film, the presence of nitride (TiN), oxynitride (TiO_xN_y), and oxide (TiO_2) phases were observed. The XPS survey spectra of 1 min etched surface of the Ti/TiN coating (Figure 1(a)) on SS exhibited characteristic Ti2p and N1s peaks at binding energies 454.5 and 397.0 eV, respectively. At 530.6 eV, a peak is observed due to the presence of O1s on the surface of the coating (Figure 1(b)) [29]. The C1s peak in the spectra (at 284.9 eV) may be attributed to the organic carbon, which is unavoidable while using an oil diffusion pump for evacuating the deposition chamber and XPS sample holding compartment [30]. Additionally, the Ar2p peak identified in the spectra of the etched surface may be attributed to adsorbed argon during

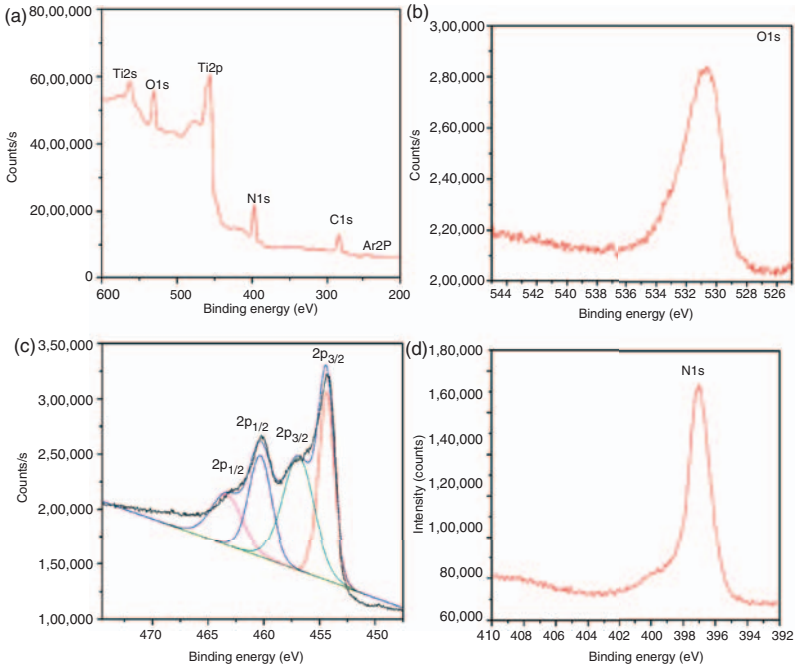

Figure 1. High resolution XPS spectra of Ti/TiN multilayers showing: (a) survey spectra, (b) O1s, (c) Ti2p scan, and (d) N1s scan.

etching or Ar species incorporated into the coating during the growth [31]. From high resolution XPS measurements of the normal surface of the films, the spin orbit doublet Ti2p1/2 and Ti2p3/2 peaks at binding energies 463.1 and 460.3 eV, respectively, were found in the Ti spectra as shown in Figure 1(c). The Ti2p3/2 peak may be deconvoluted into three components whose peaks are centered at 460.3 (I), 456.9 (II), and 454.5 (III) eV. In line with literature [32], we can easily associate these components with the Ti species present in the TiO_2, TiO_xN_y, and TiN phases, respectively. N1s spectrum showed peaks centered at 397.0 eV (Figure 1(d)). The low nitridation in the films may be attributed to high surface oxidation. The source of oxidation may be the commercial nitrogen gas, which might have contained considerable percentage of impure oxygen [33].

Although the detection efficiency of elements with low atomic-mass number such as nitrogen is low in energy dispersive spectroscopy (EDS) analysis (Figure 2), the relative compositions of Ti/TiN films are found to be 70.09 and 13.99 for Ti and N, respectively. In addition to constituent elements, 13.30% of oxygen was also detected in the EDS data. The presence of oxygen could be attributed to a very thin oxide layer formed on the surface of the film. It may also be due to an incipient corrosion process during handling of the sample. The presence of 2.62%

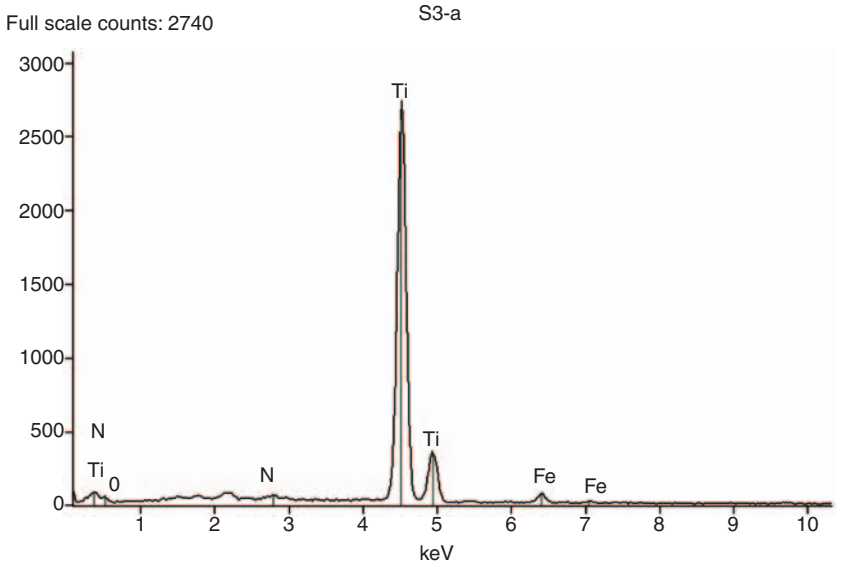

Figure 2. EDAX spectrum of Ti/TiN multilayer film.

Fe is due to substrate. The structure of the coatings was studied using powder X-ray diffraction (PXRD) by mounting the samples directly on a Philips Diffractometer, operated in reflection geometry (CuKα, 1.541 Å). The data were collected at a continuous 2θ scan rate of 1°/min or less, and were then rebinned into 2θ with steps of 0.02°. All PXRD profiles were fit by the Rietveld method (Topas), using published structure of TiN (ICSD nos. 38-1420) in literature. The pattern shown in Figure 3 exhibits reflections corresponding to TiN and Ti and the fit by the Rietveld refinement procedure to this diffraction profile confirmed the face centered cubic (FCC) structure of the film with agreement factor 0.91%. The presence of TiO_2 with weak intensity was also noticed.

The selected area electron diffraction (SAED) pattern (Figure 4) is indexed as a NaCl structure according to the observed diffraction rings. Refined crystals grow along the (1 1 1) preferred orientation in these coatings. The FCC structure of Ti/TiN shows other dotted ring patterns corresponding to the (2 0 0), (3 1 1), (2 2 0), (2 2 2), (3 3 1), and (4 2 0) reflections. The SAED pattern shows that the film is polycrystalline with B1-NaCl structure. The average crystallite size was estimated from the enlarged scanning electron micrographs (SEM) as well as from the X-ray line broadening using Scherrer's equation $D = 0.9\lambda/(\beta \cos\theta)$. The average crystallite size was found to be in the range of ~20–40 nm, with discrepancy of less than 3% between the values obtained from both the methods – SEM and X-ray. The dotted rings of the diffraction pattern are the characteristics of well-crystallized TiN phases present in

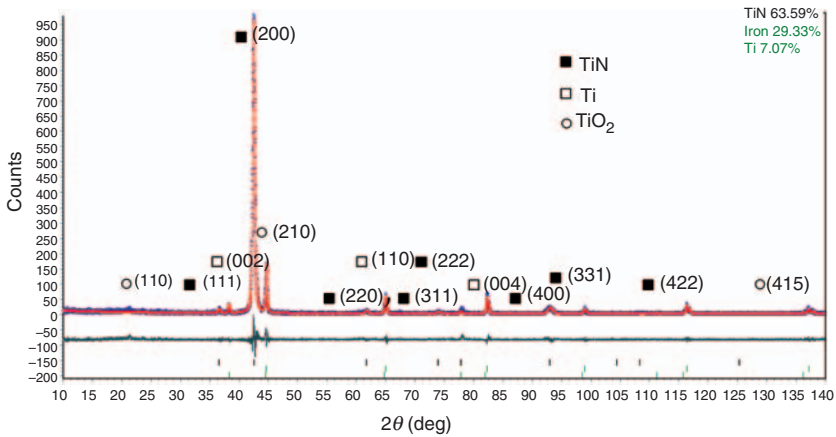

Figure 3. XRD profiles of the Ti/TiN multilayer films on mild steel: (a) observed (red), (b) refined (blue), and (c) the difference profile (black).

a polycrystalline film. This observation is in good agreement with that observed by Ikeda et al. [34]. The presence of few rings with weak intensity indicated the formation of TiO_2 phase, in addition.

Enumeration and Identification of CPB

The count of CPB amounted to 4.12×10^5 CFU/mL. CPB was identified by a biochemical test which confirmed the presence of oral microbes *Lysini bacillus* sp., *Staphylococcus* sp., *Bacillus* sp., and *Lactobacillus* sp.

Observation of Epi-fluorescence Microscope

The epi-fluorescent images in Figure 5(a)–(c), show effect of different incubation periods on the mixed culture of CPB over the TiN layer coated on SS substrate. The result indicates that the CPB initially adhere to the Ti/TiN-coated metal surface to facilitate an initial biofilm formation within 2 h. The calcium-precipitating bacterial counts were found to be increasing as 2.75×10^2, 9.0×10^2, and 1.32×10^3 for different incubation periods of 2, 24, and 48 h, respectively. It shows that as the incubation time is increased, the formation of calcium-precipitating bacterial biofilm and coverage of the metal surface is increased. The CPB play a major role in the accumulation of calcium phosphate within the film by which a biofilm formed on the coating surface. There is no marked difference in biofilm formation on TiN coating also, because

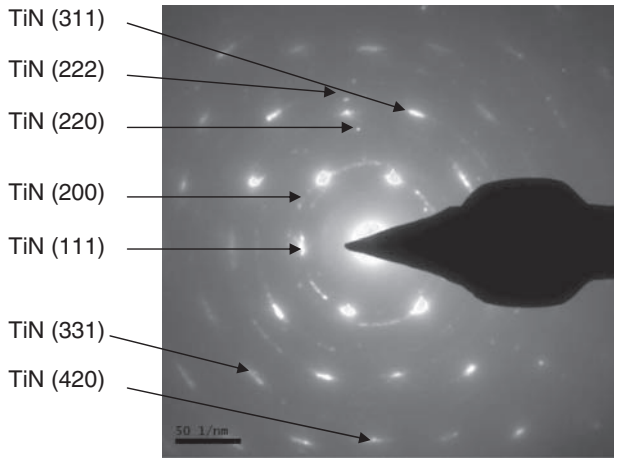

Figure 4. SAED pattern obtained for Ti/TiN multilayer film.

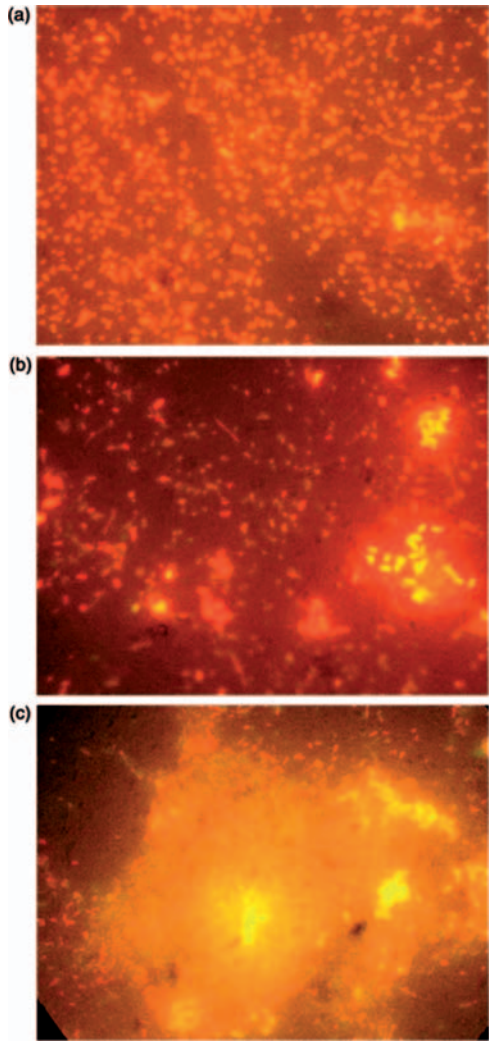

Figure 5. Epi-fluorescence micrograph of Ti/TiN multilayer with biofilm at different immersion periods: (a) 2 h, (b) 24 h, and (c) 48 h.

similar effect has been observed. SEM and AFM images taken for the Ti/TiN specimen are shown in Figure 6(a) and (b), respectively. The images clearly indicate the presence of rod-shaped CPB on the surface of the coating. Figure 6(c) shows the presence of calcium HA on the surface of the biofilm elucidated by energy dispersive X-ray analysis.

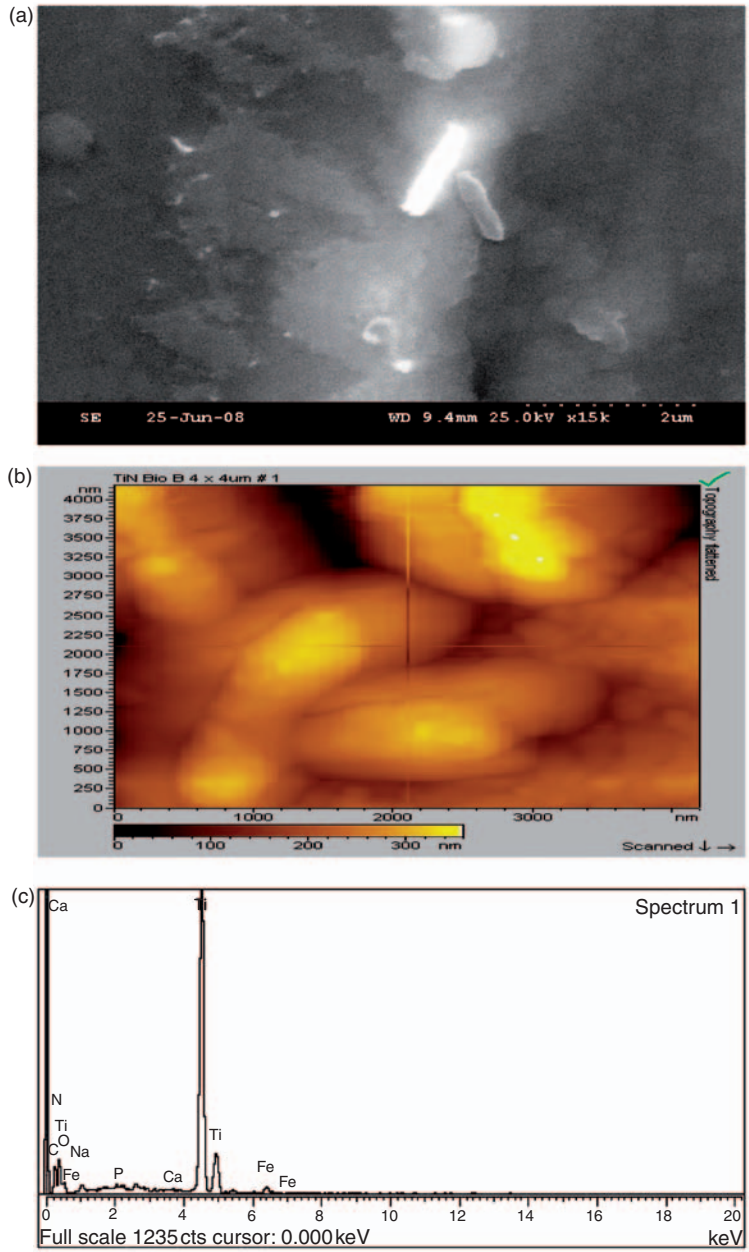

Figure 6. (a) SEM image of bacteria present on the surface of the biofilm, (b) EDAX spectrum of calcium hydroxyapatite on biofilm, and (c) AFM picture of bacteria present on the surface of the biofilm.

Hemocompatibility Studies

Platelet adhesion tests on the 316L SS surface at 60 min incubation showed larger number of the adherent platelets, with a high degree of spreading and mutual interaction (Figure 7(a)). There are only very few platelets adherent on the surface of TiN single layer coating and with Ti/TiN nanoscale multilayer specimen (Figure 7(b) and (c)), which may be due to the presence of few pin holes in the TiN layers. The disadvantage of physical vapor deposited coatings is that they inherently possess columnar microstructures leading to a large number of pores in the coatings. Platelets might have been trapped into the defective area rather than adhesion with spreading. Several reports have pointed out those surface-associated properties, such as structure, surface energy, surface charge, and surface roughness, greatly influence on the hemocompatibility of biomaterials. It is known that the isoelectric point (IEP) is approximately pH 7.4 for blood. Because mixed oxynitride phases exist at the surface of the Ti/TiN-multilayered film, the reported IEP value of its hydrated surface in air is approximately pH 4.0 [35]. When the multilayered film is exposed to the blood, the film will be negatively charged; thus, the blood elements such as blood platelets with negative charge will not adhere to the negatively charged surface easily, affecting the formation of thrombus on the surface. The lower IEP value is attributed to the good hemocompatible nature of the deposited Ti/TiN-multilayered coating in the present study.

RMS roughness value for the nanoscale multilayered Ti/TiN coating is calculated to be 7.5 nm and TiN film 42 nm whereas for the mechanically polished bare SS substrate it is very high in the order of 200 nm. A much smooth multilayer was obtained from the bare and the TiN-coated specimen. However, there exist few defects as observed from the micrograph of the Ti/TiN-multilayered coating, such as micro-particles and pin-holes. These defects may contribute to the hemolytic nature, and are of a size comparable to the red blood cells. They could possibly damage the cell membranes leading to the formation of thrombus [36]. Therefore, thrombus formation on the localized area of Ti/TiN-multilayered coating may be ascribed to its defects.

At higher magnification, it is observed that platelets were absent and only features of the coated material are present on the surface of the Ti/TiN-multilayered coatings. These results indicate that the Ti/TiN-multilayered coating shows layer improvement in the hemocompatibility more than the TiN single layer and the bare substrate.

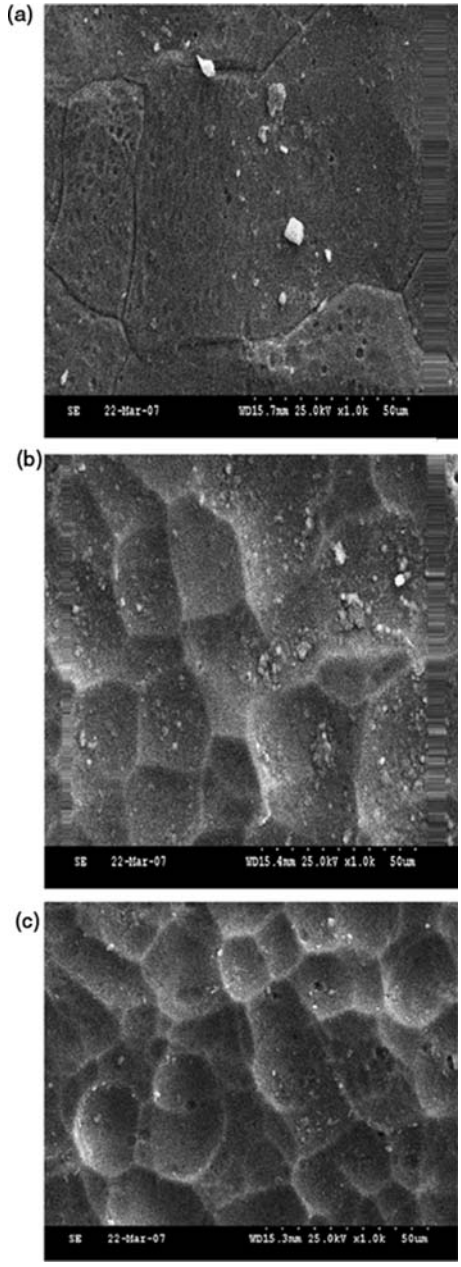

Figure 7. SEM micrograph showing the morphology of the adherent blood platelets on (a) the substrate, (b) TiN coating, and (c) Ti/TiN coating.

Electrochemical Corrosion Studies

Anodic cyclic voltammetry curves of uncoated SS substrate, Ti/TiN nanoscale multilayered film and the Ti/TiN films with biosynthesized calcium HA coating are shown in Figure 8. For the uncoated substrate, a continuous increase of the current density for the entire range of potential has been observed. A lesser rate of dissolution was shown by the sample with biocoating as inferred from the figure indicating the lowest current densities associated with the entire range of potentials studied. Typical polarization curves obtained for the corrosion behavior of the samples are shown in Figure 9. Table 1 shows the results of corrosion testing for these specimens in a simulated body fluid. The corrosion potential of the 316L SS substrate is about -0.380 V. The corrosion current I_{corr} of steel substrate is greater than those of Ti/TiN with biofilm. For the Ti/TiN nanoscale multilayer coating with biofilm, the corrosion current is reduced to 2.9×10^{-7} A/cm^2, as indicated in Table 1. Liu et al. [37], have reported that the multilayered Ti/TiN-coated specimen showed higher resistance against pitting corrosion failure with a higher breakdown potential than the TiN-coated

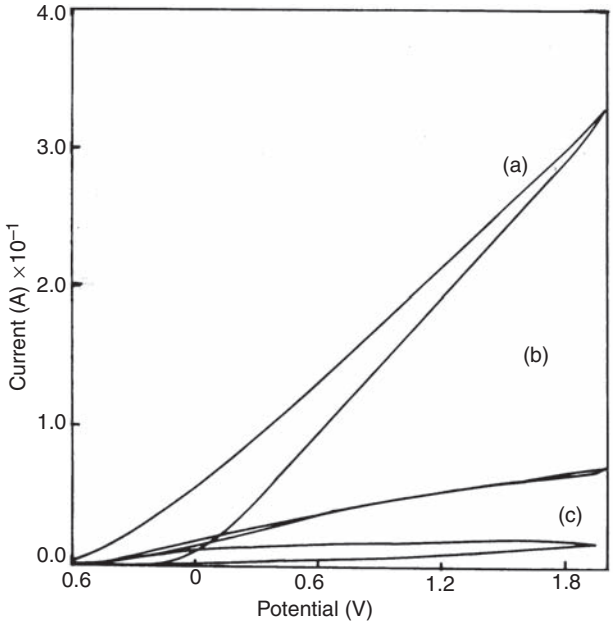

Figure 8. Cyclic voltammetry of (a) blank substrate, (b) Ti/TiN, and (c) Ti/TiN multilayer with biofilm in simulated bodily fluid.

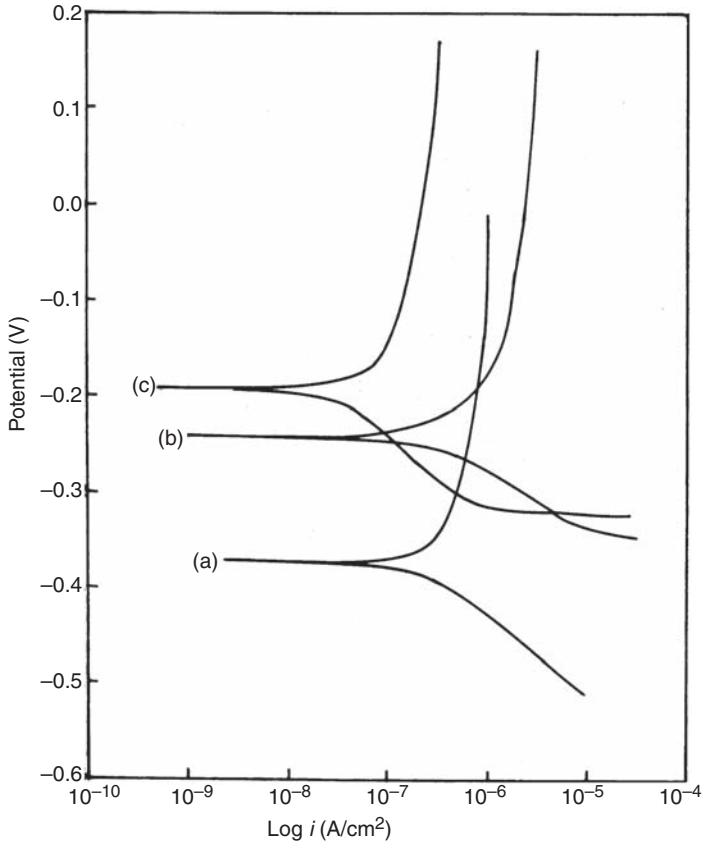

Figure 9. Polarization studies of (a) blank substrate, (b) Ti/TiN, and (c) Ti/TiN multilayer with biofilm in a simulated bodily fluid.

Table 1. Potentiodynamic polarization and electrochemical impendence data.

Sample	E_{corr} (mV)	*ba* ($vdec^{-1}$)	*bc* ($vdec^{-1}$)	I_{corr} ($\times 10^{-6}$ $A\,cm^{-2}$)	Corrosion rate	R_{ct} ($\times 10^{3}$ Ωcm^2)	C_{dl} ($\times 10^{-6}$ F/cm^2)
Bare substrate	−0.380	2.4	−0.2	4	1.9	07	1225
Ti/TiN/substrate	−0.243	0.8	−0.2	0.9	1.4	24	720
Biofilm/Ti/TiN/ substrate	−0.191	0.22	−0.09	0.29	0.3	32	462

specimen, which has been attributed to its higher compactness. Such an improvement in corrosion resistance is attributed not only to the compactness, but also to the internal microstructure. The porosity of coatings is the main factor that affects the corrosion resistance. The porosity is associated with the microstructure of the coating – the higher the packing factor the lower the porosity. For the Ti/TiN nanoscale multilayered coating, the Ti and TiN layers were deposited alternatively wherein the growth of the columnar structure of the individual TiN layer, which is detrimental to coatings used in severe corrosion environments, has been suppressed markedly. Therefore, the formation of through-coating pinhole channels is eliminated, which means that the possibility of the corrosive solution contacting the SS substrate is highly reduced.

Impedance measurements (Figure 10) were made at OCP by applying an AC signal of 10 mV in the frequency range between 0.01 Hz and 100 kHz. The double layer capacitance C_{dl} value is obtained from the frequency at which Z imaginary is maximum:

$$w(Z_{lm}\,\max) = \frac{1}{C_{dl} \times R_{ct}} \tag{1}$$

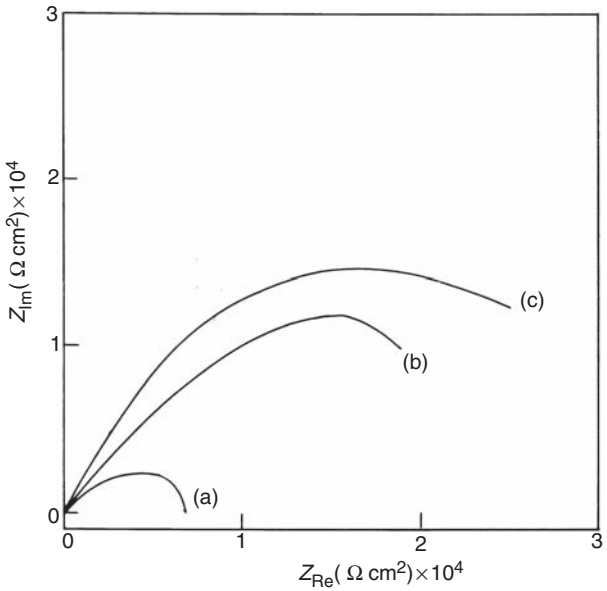

Figure 10. Nyquist plot of: (a) blank substrate, (b) Ti/TiN, and (c) Ti/TiN multilayer with biofilm in a simulated body fluid.

At higher frequencies, the interception of real axis in the Nyquist plot is ascribed to the solution resistance (R_s) and at the lower frequencies, the real axis interception gives the charge transfer resistance (R_{ct}).

When the sample is immersed in the electrolyte, the defects in the coating provide the direct diffusion path for the corrosive media. Parameters R_{ct} and C_{dl} are related to the charge-transfer reaction at the electrolyte/substrate interface. R_{ct} increases (Table 1) in the following order: 316L SS substrate < Ti/TiN < Ti/TiN with biofilm. It shows that the biofilm of calcium HA on Ti/TiN nanoscale multilayered coating has superior corrosion resistance behavior.

CONCLUSIONS

Reactive DC magnetron sputtering technique has been successfully used in depositing Ti/TiN nanoscale multilayers of thickness onto 1.5 μm 316L SS substrates. From XPS analysis it is observed that oxidation is predominant in the surface of the film. TEM SAED pattern shows the presence of a dominant well-crystallized polycrystalline state. Biofilm of calcium HA could be formed on the surface of TiN through the biomediated synthesis route. Tafel plots in simulated bodily fluid show that the corrosion rate for the specimens follows the order: 316L SS substrate > Ti/TiN > Ti/TiN with biofilm. The nanoscale multilayered Ti/TiN coating with biofilm of calcium HA has shown highly improved corrosion resistance behavior, and possesses lower passivation current density, which can be effectively used in dental implant applications.

ACKNOWLEDGMENTS

One of the authors (B.S.) thanks the Department of Science & Technology, New Delhi, for providing a research grant under SERC scheme no. SR/S1/PC/31/2008. The authors would like to thank Dr V. Swaminathan of Nanyang Technical University, Singapore for the Rietveld Refinement analysis.

REFERENCES

1. Her, H.H., Chu, H.H., Szu, J.P., Ju, L.H., Chun, C.C. and Tien, L.L. Corrosion and Cell Adhesion Behavior of Tin Coated and Ion-nitrided Titanium for Dental Applications, *Appl. Surf. Sci.*, 2005: **244**: 252–256.
2. Sundgren, J.E. Structure and Properties of TiN Coatings, *Thin Solid Films*, 1985: **128**: 21–44.

3. Watari, F., Tamura, Y., Yokoyama, A., Uo, M. and Kawasaki, T. Mechanical Properties and Biocompatibility of Surface-nitrided Titanium for Abrasion Resistant Implant, *Key Eng. Mater.*, 2004: **254/256**: 873–876.
4. Czarnowska, E., Wierchon, T. and Maranda Nieabala, A. Properties of the Surface Layers on Titanium Alloy and Their Biocompatibility in Vitro Tests, *J. Mater. Proc. Technol.*, 1999: **190**: 92–93.
5. Wan, Z.N., Dorr, L.D., Woodstone, T., Ranawat, A. and Song, M. Effect of Stem Stiffness and Bone Stiffness on Bone Remodeling in Cemented Total Hip Replacement, *J. Arthroplasty*, 1999: **14**: 149–159.
6. Hench, L.L. Bioceramics: From Concept to Clinic, *J. Am. Ceram. Soc.*, 1991: **74**: 1487–1510.
7. Aoki, H. (1994). *Medical Applications of Hydroxyapatite*, St. Louis, Tokyo, Ishiyaku Euro America. Inc., pp. 1–12.
8. Lacefield, W.R. Hydroxyapatite Coatings, *Ann. N.Y. Acad. Sci.*, 1988: **523**: 72–80.
9. Li, T.T., Lee, J.H., Kobayashi, T. and Aoki, H. Hydroxyapatite Coating by Dipping Method, and Bone Bonding Strength, *J. Mater. Sci. Mater. Med.*, 1996: **7**: 355–357.
10. Locardi, B., Pazzaglia, U.E., Gabbi, C. and Profilo, B. Thermal Behaviour of Hydroxyapatite Intended for Medical Applications, *Biomaterials*, 1993: **14**: 437–441.
11. Yankee, S.J., Platka, B.J., Luckey, H.A. and Johnson, W.A. (1990). Process for Fabricating HA Coatings for Biomedical Applications, Thermal Spray Research and Applications, In: *Proceedings of the 3rd Annual Thermal Spray Conference*, Long Beach, California, 20–25 May, p. 433–438.
12. Raemdonck, W.V., Ducheyne, P. and Meester, P.D. Auger Electron Spectroscopic Analysis of Hydroxyapatite Coating on Titanium, *J. Am. Ceram. Soc.*, 1986: **63**: 381–384.
13. Jaffe, W.L. and Scott, D.F. Current Concepts Review – Total hip Arthroplasty with Hydroxyapatite-coated Prostheses, *J. Bone Joint Surg.*, 1996: **78**: 1918–1934.
14. Ong, J.L. and Lucas, L.C. Post-deposition Heat Treatments for Ion Beam Sputter Deposited Calcium Phosphate Coatings, *Biomaterials*, 1994: **15**: 337–341.
15. Yoshinari, N., Ohtsuka, Y. and Derand T. Thin Hydroxyapatite Coating Produced by the Ion Beam Dynamic Mixing Method, *Biomaterials*, 1994: **15**: 529–535.
16. Lin, J.H.C., Liu, M.L. and Ju, C.P. Structure and Properties of Hydroxyapatite-bioactive Glass Composites Plasma Sprayed on Ti6Al4V, *J. Mater. Sci. Mater. Med.*, 1994: **5**: 279–283.
17. Brossa, F., Cigada, A., Chiesa, R., Paracchini, L. and Consonni C. Adhesion Properties of Plasma Sprayed Hydroxylapatite Coatings for Orthopaedic Prostheses, *Biomed. Mater. Eng.*, 1993: **3**: 127–136.
18. Bortz, S.A. and Onesto, E.J. Flame-sprayed Bioceramics, *Am. Ceram. Soc. Bull.*, 1975: **52**: 89–93.
19. Layrolle, P., Ito, A. and Tateishi, T. Sol–Gel Synthesis of Amorphous Calcium Phosphate and Sintering into Microporous Hydroxyapatite Bioceramics, *J. Am. Ceram. Soc.*, 1998: **81**: 1421–1428.

20. Müllera, F.A., Müllera, L., Caillardb, D. and Confortoc, E. Preferred Growth Orientation of Biomimetic Apatite Crystal, *J. Cryst. Growth*, 2007: **304**: 464–471.
21. Habibovic, P., Barrère, F., Clemens, A., Blitterswijk, V., Groot, K.D. and Layrolle, P. *J. Am. Ceram. Soc.*, 2002: **85**: 517–522.
22. Müller, L., Conforto, E., Caillard, D. and Frank, A. Biomimetic Apatite Coatings – Carbonate Substitution and Preferred Growth Orientation, *Biomol. Eng.*, 2007: **24**: 462–466.
23. Tas, A.C. Synthesis of Biomimetic Ca-hydroxyapatite Powders at 37°C in Synthetic Body Fluids, *Biomaterials*, 2000: **21**: 1429–1438.
24. Yong, P., Macaskie, L.E., Sammons, R.L. and Marquis, P.M. Synthesis of Nanophase Hydroxyapatite by a *Serratia* sp. from Waste-water Containing Inorganic Phosphate, *Biotechnol. Lett.*, 2004: **26**: 1723–1730.
25. Black, J. (1999). *Fundamentals of Biocompatibilities*, New York, Marcel Dekker, pp. 444–457.
26. Jasen, J.A., Van der Waerden, J.P. and De Groot, K. Development of a New Percutaneous Access Device for Implantation in Soft Tissues, *J. Biomed. Mater. Res.*, 1991: **25**: 1535–1545.
27. Cappucino, J. and Sherman, N. (2002). *Microbiology: A Laboratory Manual*, 6th edn, San Francisco, Benjamin Cummings, pp. 1–21.
28. Fusayama, T., Katayori, T. and Nomoto, S. Corrosion of Gold and Amalgam Placed in Contact with Each Other, *J. Dent. Res.*, 1963: **42**: 1183–1197.
29. Zhao, J., Garza, E.G., Lam, K. and Jones, C.M. Comparison Study of Physical Vapor-deposited and Chemical Vapor-deposited Titanium Nitride Thin Films Using X-ray Photoelectron Spectroscopy, *Appl. Surf. Sci.*, 2000: **158**: 246–251.
30. Mushar, J.N. and Gordon, R.G. Atmospheric Pressure Chemical Vapor Deposition of Titanium Nitride from Tetrakis(diethylamido) Titanium and Ammonia, *J. Electrochem. Soc.*, 1996: **143**: 736–744.
31. Deenamma, V.K., Mohan Rao, G., Balasubramanian, T.V. and Sanjiv, K. Preparation and Characterization of TiN Films by Electron Cyclotron Resonance (ECR) Sputtering for Diffusion Barrier Applications, *Mater. Sci. Eng*. B, 2001: **83**: 242–248.
32. Piscanec, S., Ciacchi, L.C., Vesselli, E. et al. Bioactivity of TiN-coated Titanium Implants, *Acta Mater.*, 2004: **52**: 1237–1245.
33. Wu, H.Z., Chou, T.C., Mishra, A. and Gujrathi, S.C. Characterization of Titanium Nitride Thin Films, *Thin Solid Films*, 1990: **191**: 55–67.
34. Ikeda S., Gilles, S. and Chenevier, B. Electron Microscopy Analysis of the Microstructure of Ti1–*x*Al*x*N Alloy Thin Films Prepared Using a Chemical Vapour Deposition Method, *Thin Solid Films*, 1998: **315**: 257–262.
35. Jones, M.I., McColl, I.R., Grant, D.M., Parker, K.G. and Parker, T.L. Haemocompatibility of DLC and TiC-TiN Interlayers on Titanium, *Diamond Relat. Mater.*, 1999: **8**: 457–462.
36. Stefano, P., Lucio, C.C., Erik, V. and Giovanni, C. Bioactivity of TiN-coated Titanium Implants, *Acta Mater.*, 2004: **52**: 1237–1245.
37. Chenglong, L., Dazhi, Y., Guoqiang, L. and Min, Q. Corrosion Resistance and Hemocompatibility of Multilayered Ti/TiN-coated Surgical AISI 326L Stainless Steel, *Mater. Lett.*, 2005: **59**: 3813–3819.